

Article

Lignin Nanosphere-Supported Cuprous Oxide as an Efficient Catalyst for Huisgen [3+2] Cycloadditions under Relatively Mild Conditions

Zidan Zhou ¹, Xinwen Peng ^{1,*}, Linxin Zhong ^{1,*}, Xuehui Li ² and Runcang Sun ³

¹ State Key Laboratory of Pulp and Paper Engineering, South China University of Technology, Guangzhou 510641, China; zidanzhou@aliyun.com

² School of Chemistry and Chemical Engineering, South China University of Technology, Guangzhou 510641, China; cexhli@scut.edu.cn

³ Beijing Key Laboratory of Lignocellulosic Chemistry, Beijing Forestry University, Beijing 100083, China; rcsun3@bjfu.edu.cn

* Correspondence: fexwpeng@scut.edu.cn (X.P.); lxzhong0611@scut.edu.cn (L.Z.)

Received: 18 April 2018; Accepted: 13 June 2018; Published: 2 July 2018



Abstract: In this work, low-cost lignin nanospheres were fabricated and further applied as an efficient and sustainable support for preparing cuprous oxide (Cu₂O) “green” catalyst by using electrospaying technology. The unalloyed lignin, a special three-dimensional molecular structure, was successfully processed into uniform nanospheres under an electrospaying condition. The synthesized lignin-supported Cu₂O catalyst had a well-defined nanosphere structure, and Cu₂O nanoparticles with sizes less than 30 nm were supported by exposed layers of lignin nanospheres. There were C–O–Cu bonds formed between the lignin nanospheres and the metallic nanoparticles. The lignin nanospheres and the lignin nanosphere-supported catalyst were characterized by utilizing XRD, SEM, TEM, XPS, EDS, and TGA. The immobilization of Cu₂O nanoparticles on the lignin nanospheres was beneficial for dispersion of the Cu₂O nanoparticles and preventing their aggregation, which could cause catalyst deactivation, which favored the Huisgen [3+2] cycloaddition reaction. The triazole synthesis results indicated that the lignin nanosphere-supported Cu₂O catalyst had a high catalytic performance with 99% yield under solvent-free conditions. Furthermore, the as-synthesized catalyst could be recycled for four times without significantly losing its catalytic activity.

Keywords: electrospaying technology; lignin; nanospheres; solvent-free reaction

1. Introduction

“Click” chemistry has a wide scope, gives high yields, and forms irreversible carbon–heteroatom and carbon–carbon bonds [1]. It uses only the most practical and reliable chemical reactions to connect a diversity of structures bearing a wide variety of functional groups [2]. Therefore, it has attracted much attention in many research areas, such as catalyst design, polymer synthesis, material science, synthesizing libraries of compounds, and drug development [3]. Monovalent copper-mediated azide–alkyne Huisgen [3+2] cycloaddition is a highly typical and important “click” reaction [4]. It involves the ligation of azides and terminal alkynes to generate triazoles, and usually needs a copper salt in conjunction with a base. The catalyst can be a Cu(I) salt or Cu(I) generated in situ by the reduction of Cu(II) salts, usually in organo-aqueous media [5], and allows facile and reliable production of 1,4-disubstituted 1,2,3-triazoles.

Nowadays, there is a growing interest in the synthesis of environmentally benign catalysts [6] because of their added advantages, such as requiring mild reaction conditions and being simple to recover and regenerate, as well as being environmentally friendly [7]. It is desirable to

develop high-performance and “green” heterogeneous catalysts for “click” chemistry. Recently, the development of Cu-based heterogeneous catalysts with the presence of copper or cuprous oxide nanoparticles has significantly increased catalytic activity for the construction of triazole molecules, owing to the enhanced surface area of copper or cuprous oxide and unique catalyst structure–activity relationships [8–10]. The supported catalysts are simple to prepare. The inexpensive catalysts are practical for their applications. Moreover, the immobilization of small Cu or Cu₂O nanoparticles on supports makes the catalyst easily reusable with excellent recyclability performance, largely reduces nanoparticle leakage, and avoids environmental hazards. Currently, the most commonly used solid supports for heterogeneous catalysts include silica [11], zeolites [12], graphene [13], magnetic materials [14], and soluble and insoluble polymers [15]. Furthermore, various other supports have been used in different catalytic reactions [16–21]. However, some of these supports of the heterogeneous catalysts may not be sufficient in the near future. As a result, it is crucial to switch to cheap and biorenewable resources. Natural biopolymers [22–24] have been considered as attractive candidates to create high-performance biobased catalysts due to their abundance, renewability, biodegradability, and low cost [25]. Lignin is one of the most important biopolymers from renewable resources, owing to its abundance (being the second most plentiful plant biopolymer on the earth, after cellulose). The production of lignin is over 50 million tons worldwide annually, while its utilization is rather limited except for its use in biochar or activated carbon [26]. Therefore, lignin is a desirable raw material for fabricating value-added products for various applications. Recently, the synthesis of lignin-based functional materials and their potential applications have attracted much attention, such as anode materials for lithium-ion batteries [27], supercapacitors [28], and electrocatalysts [29]. Furthermore, lignin derivatives exhibit interesting and attractive abilities in improving the performance of photovoltaic devices [30]. As a heterogeneous and rigid polymer of phenolic nature, it is the only biomass that is based on aromatic units. It is composed of phenylpropane, including *p*-coumaryl alcohol, coniferyl alcohol, and sinapyl alcohol, which makes it highly polar with a large amount of hydroxyl groups. Moreover, typical C–O links of the lignin are β -O-4, α -O-4, and 4-O-5; and C–C links are β -5, 5-5, β -1, and β - β linkages [31–34]. It has hydroxylic groups and aromatic methoxy, carboxylic, carbonylic, and ethereal moieties. Most importantly, lignin owns three-dimensional molecular structures. These make lignin an efficient and stable ligand for the preparation of biocatalysts.

Electrospinning is a relatively convenient and versatile strategy to produce nanofibers from polymer solutions or blends. However, lignin possesses complex three-dimensional structures with various types of functional groups. The lignin is formed by oxidative coupling of the main three kinds of lignin precursors; the reaction sites abound upon forming of the body polymers. The special architectural structures of lignin have led to little success in creating absolute lignin electrospinning nanofibers. Current strategies for using lignin in electrospinning nanofibers focus on integrating it with other natural or synthetic polymers; for instance, Kai et al. [35] engineered nanofibrous composites with different lignin mass fractions into lignin–polymethylmethacrylate by electrospinning technology. Interestingly, we found that the special molecular structure of lignin made it easy to be processed into nanospheres when electrospaying lignin precursor solution at an appropriate concentration in DMF solvent under a determined voltage condition. The inherent phenolic hydroxyl, carboxylic, and carbonylic groups in lignin molecules are beneficial for the adsorption of Cu ions, among others, to load and coordinate [36,37], and the three-dimensional molecular structure contributes to making lignin a stable and favorable support for catalysts.

Herein, we report a novel straightforward method to fabricate lignin nanospheres in quantity (in the grams scale) by utilizing electrospaying technology. Then, we successfully exploit it as an effective support for Cu₂O nanoparticles for preparing a high-performance cuprous oxide heterogeneous catalyst. Above all, lignin and monovalent copper could form Cu₂O@L composites owing to the abundant carbon–oxygen bonds in lignin molecules. Meanwhile, the strongly polar phenolic hydroxyl and alcoholic hydroxyl groups contributed to its reducing property [38,39], which

avored the reduction of cupric sulfate in aqueous solution for the preparation of cuprous oxide catalyst. In particular, Cu₂O@L was investigated to catalyze a series of Huisgen “click” reactions and showed excellent activity for 1,2,3-triazole syntheses. The reactions proceeded under air conditions in the absence of organic solvents, without adding any base or external heating, which made the method to be a simple, powerful, and environmentally benign alternative. Furthermore, the catalytic performance of the Cu₂O@L was researched in terms of a series of azides and terminal alkynes. As compared with other copper-mediated Huisgen “click” cycloaddition reactions, “click” reactions using the Cu₂O@L exhibited a higher yield and required a shorter reaction time and relatively mild reaction conditions.

2. Materials and Methods

The alkali lignin ($M_w = 6000$) was purified from poplar wood pulping black liquor using acid treatment; the black liquor was provided by Shuntai Co., Ltd. (Changsha, Hunan, China). Cu₂O (~30 nm) for comparison was purchased from Shandong Xiya Chemical Reagent Co., Ltd. (Linyi, Shandong, China). All the chemicals were used as received without further purification.

2.1. Electrospraying Lignin Nanospheres

In a typical process, lignin solution with a concentration of 35 wt % was prepared by dissolving 0.9 g lignin into 1.1 g DMF liquid solution in a flask. The mixture liquid was then stirred at room temperature for 2 h until the lignin was completely dissolved. The electrospraying setup used in this study consisted of a syringe and needle (ID = 0.84 mm), high voltage supply, a ground electrode, and a collector (stainless steel sheet). A syringe pump connected to the syringe controlled the flow rate. The lignin nanospheres were obtained by electrospraying at a positive voltage of 15 kV and a negative voltage of 1 kV, with a tip-to-collector distance of 15 cm and a solution flow rate of 0.75 mL/h. The procedure was carried out at 25 °C and 60% ambient humidity. The lignin nanospheres were stripped down from aluminum paper and then dried in an oven. Furthermore, the electrosprayed lignin nanospheres were preliminarily heated at 280 °C in air for 2 h and then were heated to 800 °C with a heating rate of 1 °C/min. Finally, the nanospheres were held for 30 min under N₂ atmosphere in a tube furnace to obtain lignin carbon nanospheres.

2.2. Preparation of Cu₂O@L

The preparation of Cu₂O@L used the methods as follows: In a 50 mL test tube, 10 mL of double-distilled water was added into the test tube and stirred at room temperature. 500 mg lignin nanospheres were added to form a suspension. Then, 10 mL (2%, *w/v*) of aqueous copper sulphate solution was added into the suspension with stirring for an hour. This process was carried out in N₂ atmosphere to eliminate the dissolved oxygen present in the solution. An aqueous solution of hydrazine hydrate (4 M) as the main reducing agent was added to reduce the copper sulfate to Cu₂O nanoparticles sufficiently. After 2 h of continuous stirring, the catalyst was separated using a centrifuge (10,000 rpm, 10 min) and washed with double-distilled water for three times to remove the untrapped particles and ions. The wet sample was then dried in an oven to obtain Cu₂O@L.

2.3. Catalytic Performance Test

The catalytic ability of Cu₂O@L was evaluated by the synthesis of triazoles from alkyl azide and alkyne. 1.2 mmol of alkyne, 1.0 mmol of alkyl azide, and 20 mg (1.2 mol %) Cu₂O@L were added into a reaction tube under organic solvent-free conditions. Then, the reaction mixture was stirred for 3 h at room temperature. After the reaction, the product was separated by ethyl acetate extraction from Cu₂O@L, and the catalyst was recovered by filtration or centrifugation (8000 rpm, 10 min) for reuse. The products were further purified by column chromatography on silica gel using ether/ethyl acetate (5:1) as the eluent. The triazoles were obtained after solvent evaporation and the yield of the products was calculated.

For the practical applications of such heterogeneous systems, the lifetime of the catalyst is a very significant factor for evaluation of catalyst performance. Therefore, the number of cycles and the

catalytic activity in terms of reaction yield using the recycled catalyst were also studied. After the completion of the first reaction, the product was extracted using ethyl acetate and the catalyst was recovered by simple centrifugation and dried at room temperature. Then, a fresh reaction was performed with new reactants, under the same conditions.

2.4. Analyses

All ^1H spectra of the products were recorded on a FT-NMR (600 MHz, Bruker Corp., Karlsruhe, German) spectrometer, and ^{13}C spectra were recorded on a Bruker FT-NMR (151 MHz). NMR chemical shifts are given as δ values (ppm) with reference to TMS as the internal standard. FTIR spectra were recorded on a Bruker Nicolet 6700 FTIR spectrophotometer in the range of $400\text{--}4000\text{ cm}^{-1}$ using KBr pellets. The Cu content was determined by a Hitachi Z-2000 AAS (Tokyo, Japan). SEM images were recorded on a Zeiss EVO-18 (Oberkochen, Germany) operating at 10 kV, and TEM images were recorded on a JEM-2100 (HR) TEM (JEOL, Tokyo, Japan) working at 200 kV. The fluorescence images were acquired using a LSCM (Leica TCS SP5, Wetzlar, Germany) equipped with a diode laser (405 nm), using a $100\times$ oil objective with numerical aperture of 1.40, and three samples were observed under the same conditions. The UV–vis–NIR absorption spectrum of Cu_2O was acquired with a PerkinElmer Lambda 750 spectrophotometer (Waltham, MA, USA). FL were taken on a FLS-980 spectrometer (Edinburgh Instruments, Ltd., Edinburgh, UK). The samples were excited by a pulse laser (405 nm). An appropriate filter was also used before the PMT to cut off any other stray light. Topographic and phase images of samples were obtained using an AFM (Bruker Dimension Fastscan) in tapping mode. XRD measurements were carried out at room temperature using a Bruker D8 Advance X-ray powder diffractometer with Ni-filtered $\text{Cu-K}\alpha$ radiation ($\lambda = 0.154\text{ nm}$) from $5^\circ\text{--}80^\circ$. XPS measurements were performed on an Axis Ultra DLD instrument using $\text{Al-K}\alpha$ radiation ($h\nu = 1486.6\text{ eV}$) with contaminated C as an internal standard ($\text{C } 1s = 284.6\text{ eV}$). EDS was measured with a Horiba XMAX X-ray energy dispersive spectroscope that was attached to the Oxford Instruments (Abingdon, UK). The size and the size distribution of $\text{Cu}_2\text{O}@L$ were measured by dynamic light scattering on a Nano-Zetasizer (Zetasizer NanoZS, Malvern Instruments Ltd., Worcestershire, UK) at 25°C under a scattering angle of 173° at $\lambda = 633\text{ nm}$. TGA (Q500, TA Instruments, New Castle, DE, USA) was carried out in an aluminum crucible by heating to 650°C at a heating rate of $20^\circ\text{C min}^{-1}$ with a nitrogen flow of 25 mL min^{-1} .

3. Results

3.1. Characterization of the Electrosprayed Lignin Nanosphere and $\text{Cu}_2\text{O}@L$

As shown in Figure S1, the concentration of the lignin solution shows a significant influence on the lignin morphology under the electrospraying condition. When the concentration of the lignin solution is 25%, 35%, or 45% (w/w), electrosprayed lignin exhibits a nanosphere shape (Figure S1a–c). Under these concentration conditions, the surface tension is greater than the electric force, which plays a key role on the nanospherical shape of lignin. However, the electrosprayed lignin exhibits the similar fiber morphology when the lignin concentration is higher than 55%, due to lignin molecular chains twining around each other (Figure S1d). As compared with the electrosprayed lignin at other concentrations, the lignin nanosphere at the concentration of 35% solution had a more uniform morphology and therefore was chosen for further studies.

The as-prepared electrosprayed lignin nanospheres show a regular spherical morphology with a diameter less than $1\text{ }\mu\text{m}$ for the most part (Figure 1a). From the SEM images, the sizes of lignin nanospheres show the average size of $605 \pm 5\text{ nm}$. As shown in Figure 1b, $\text{Cu}_2\text{O}@L$ shows a “raspberry” morphology. Furthermore, the spherical morphology of the electrosprayed lignin nanosphere still remains after carbonization at 800°C under N_2 atmosphere (Figure 1c). The reason for this is that the good rigid and three-dimensional molecular structure obviously maintains its volume unchanged before and after the carbonization process. The EDS of $\text{Cu}_2\text{O}@L$ illustrates that there are C, O, and Cu elements in the catalyst (Figure 1d). Figure 1e shows the EDS mapping image with all the elements of

$\text{Cu}_2\text{O}@L$, while Figure 1f–h shows the EDS mapping images of the C, O, and Cu elements, respectively. The SEM and EDS results showed that the $\text{Cu}_2\text{O}@L$ was a spherical structure containing the Cu element. Furthermore, the Cu concentration of the catalyst is confirmed to be 7.76% by AAS.

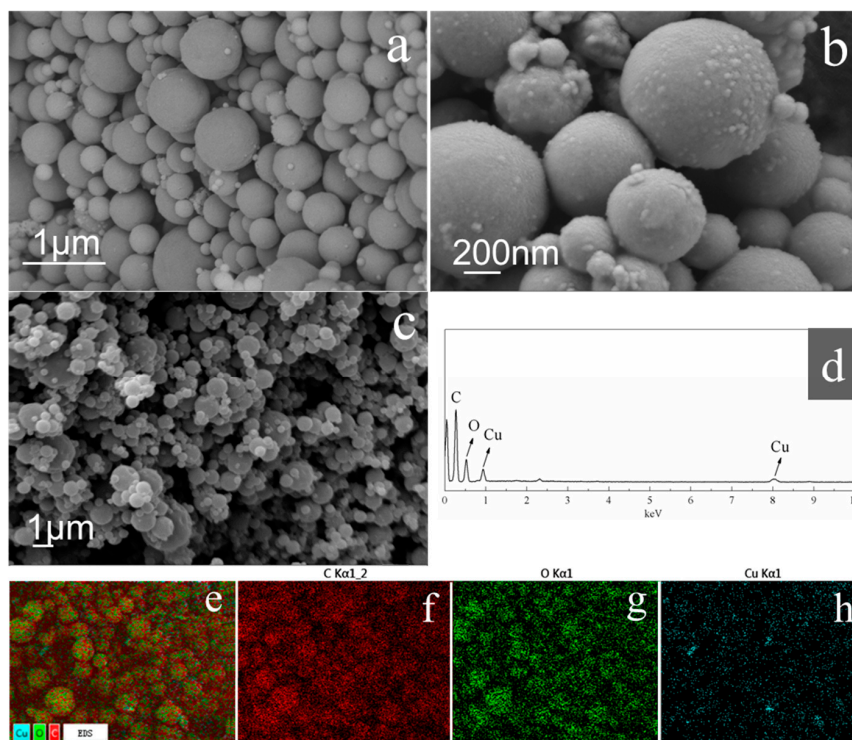


Figure 1. SEM images of lignin nanospheres and $\text{Cu}_2\text{O}@L$: (a) electrospayed lignin nanospheres; (b) $\text{Cu}_2\text{O}@L$; (c) lignin nanosphere after carbonization at 800 °C under N_2 atmosphere; (d) the EDS of $\text{Cu}_2\text{O}@L$; (e) EDS mapping images of C, O, and Cu elements; and (f) C element, (g) O element, and (h) Cu element EDS mapping, respectively.

The morphology of the electrospayed lignin nanospheres and $\text{Cu}_2\text{O}@L$ were further studied using LSCM. As shown in Figure 2a, the raw lignin has an irregular shape and good fluorescence characteristic, which is attributed to its molecular structure containing repeated units of phenylpropane. Interestingly, as compared with the electrospayed lignin nanospheres (Figure 2b), $\text{Cu}_2\text{O}@L$ shows weaker fluorescence (Figure 2c). Fluorescence spectrums of lignin, lignin nanospheres, and $\text{Cu}_2\text{O}@L$ were further investigated, which were in accordance with the results of LSCM. The lignin nanospheres show stronger fluorescence intensity than raw lignin. This is probably because the aggregation-induced emission appears among lignin molecules as the lignin is processed into nanospheres by electrospaying. The Cu_2O nanoparticles can lead to fluorescent quenching of lignin (Figure 2d), and energy transfer from lignin to Cu_2O nanoparticles occurs owing to some overlap between the emission wavelength range of lignin (420–700 nm) and the absorption wavelength of Cu_2O (400–900 nm) (Figure 2e). Furthermore, the interaction of phenolic hydroxyl groups and carbon–oxygen and cuprous bonds destroying conjugated structures or clusters of the carbonyl groups in lignin molecules [40] may result in the weakening of the characteristic fluorescence of the lignin and an obvious blue-shift of the luminescent spectrum of $\text{Cu}_2\text{O}@L$. Aggregation-induced emission of lignin nanospheres that were prepared by electrospaying is observed (Figure 2f), similarly to the phenomenon of lignin derivatives reported by Qiu and coworkers [41].

Figure 2 shows TEM and high-resolution TEM (HRTEM) images of $\text{Cu}_2\text{O}@L$ as well. The diameter of the electrospayed lignin nanospheres is less than 1 μm for the most part and some nanoparticles are present on their surfaces, as illustrated in Figure 2g. Noting that the Cu_2O are irregular in shape with

the average size of 20 ± 2 nm (Figure 2h). The HRTEM image (Figure 2i) shows that the lattice spacing of the nanoparticles is about 0.24 nm [42], which is in agreement with the crystal lattice theoretical value for the (111) planes of Cu_2O . The result indicates that the nanoparticles on lignin containing the Cu element are Cu_2O . All these results show that small Cu_2O nanoparticles have been successfully loaded onto the surfaces of the lignin nanospheres.

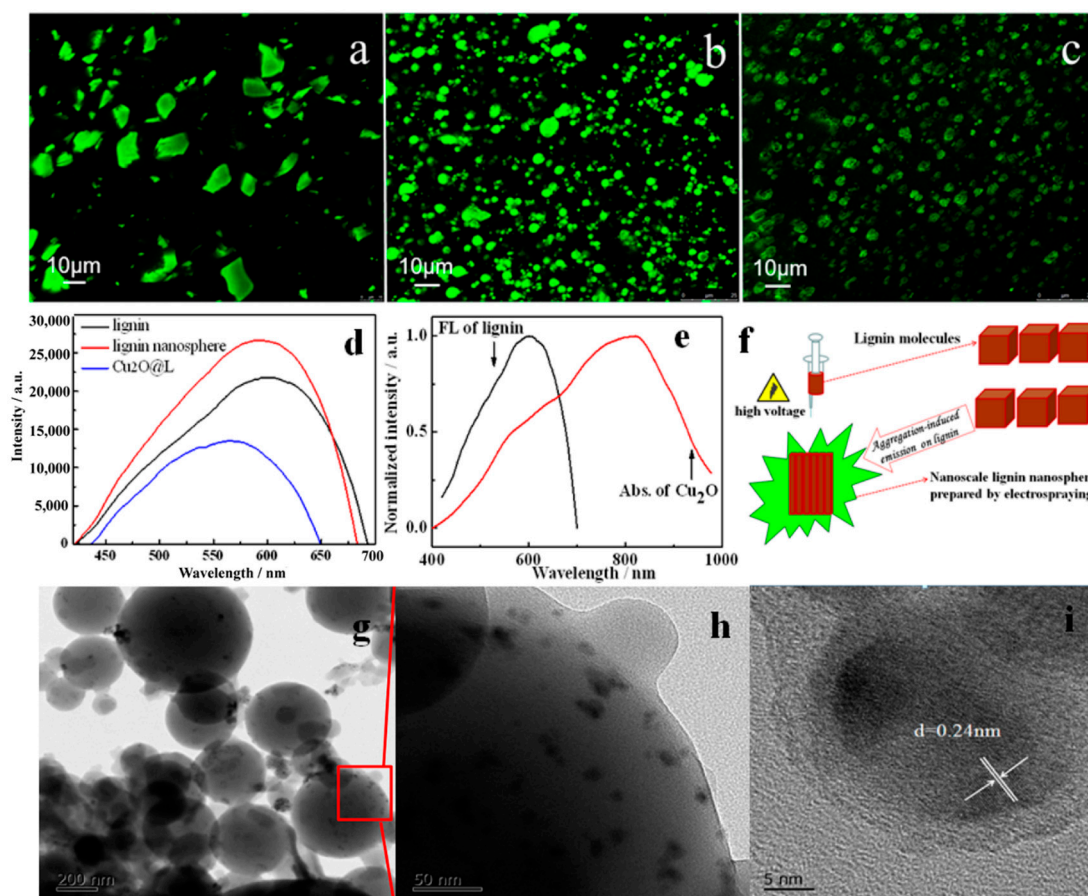


Figure 2. LSCM images, fluorescence spectra, UV-vis-NIR absorption, and TEM images of samples: (a) LSCM image of raw lignin; (b) LSCM image of lignin nanospheres; (c) LSCM image of raw $\text{Cu}_2\text{O}@L$; (d) fluorescence spectra of lignin, lignin nanospheres, and $\text{Cu}_2\text{O}@L$; (e) UV-vis-NIR absorption of Cu_2O and lignin; (f) proposed aggregation-induced emission of lignin nanospheres prepared by electro spraying; (g) TEM image of $\text{Cu}_2\text{O}@L$; (h) the expansion of a certain part of image of g, and (i) HRTEM image of the nanoparticles on lignin nanospheres.

As shown in Figure 3, height map images of AFM demonstrate the spherical shape of the electro sprayed lignin nanospheres (Figure 3a,b) and $\text{Cu}_2\text{O}@L$ (Figure 3e,f). Figure 3c shows the defective surface of the lignin nanosphere, which may contribute to it being a favorable catalyst support for preparing the high-performance lignin-based catalyst. There are two phases of $\text{Cu}_2\text{O}@L$ (Figure 3g), indicating Cu_2O being successfully loaded onto the lignin nanospheres. Besides, the 3D images of AFM (Figure 3d,h) also prove the spherical structures of the lignin nanospheres and $\text{Cu}_2\text{O}@L$. The catalyst $\text{Cu}_2\text{O}@L$ exhibits a nanoscale particle size mainly ranging from 100 to 1000 nm, which appears as a large peak at a size of around 600 nm (Figure S2). The particle-size analysis is in accordance with SEM, TEM, and the AFM results mentioned above.

The crystal structure of $\text{Cu}_2\text{O}@L$ was confirmed by XRD patterns. As shown in Figure 4a-1, the dispersion peak at $2\theta = 30\text{--}40^\circ$ is a typical XRD diffraction pattern of noncrystalline lignin. Because the overlap peak of the lignin diffraction peaks heighten at 29° , 36° , and 42° of Cu_2O [43], all of the

sharp diffraction peaks ($2\theta = 29^\circ, 36^\circ, 42^\circ, 62^\circ,$ and 74°) can be indexed to the face-centered cubic structure of Cu_2O (JCPDS file: 65-3288) (Figure 4a-2). There are still XRD diffraction peaks of Cu_2O from the reused $\text{Cu}_2\text{O}@L$ (Figure 4a-3). The XRD results are consistent with the results of HRTEM, indicating the successful loading of Cu_2O onto the lignin nanospheres.

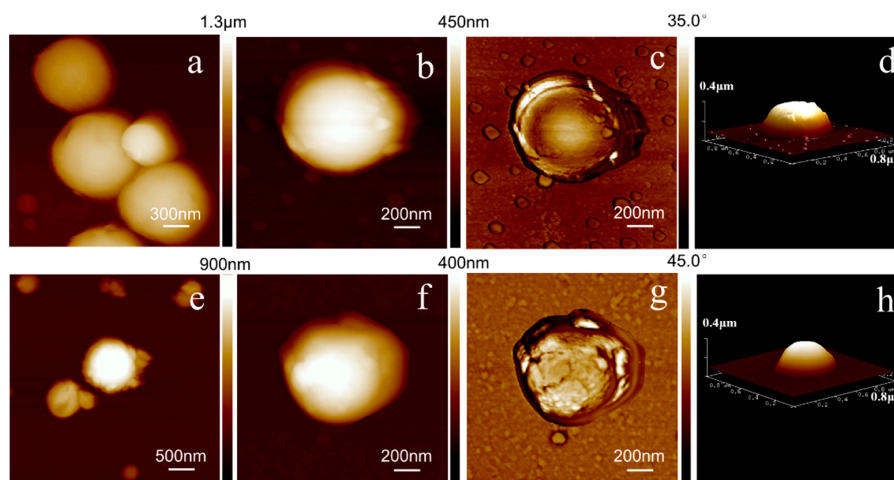


Figure 3. AFM images of the electrospayed lignin nanospheres and $\text{Cu}_2\text{O}@L$: (a,b) height map images of the lignin nanospheres; (c) phase diagram of the electrospayed lignin nanosphere; (d) 3D image of the electrospayed lignin nanosphere; (e,f) height map images of $\text{Cu}_2\text{O}@L$; (g) phase diagram of $\text{Cu}_2\text{O}@L$; (h) 3D image of $\text{Cu}_2\text{O}@L$.

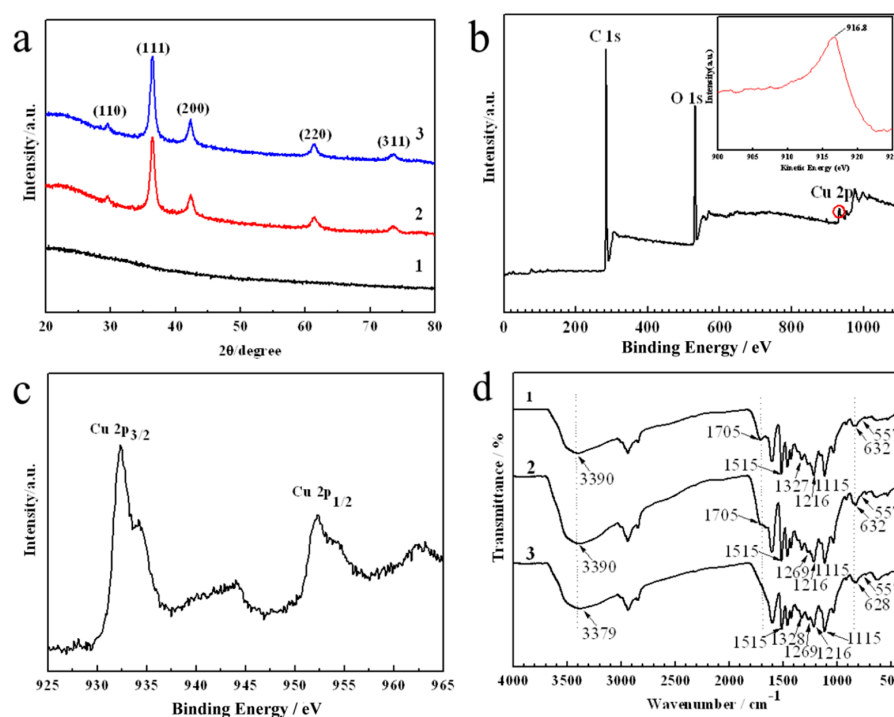


Figure 4. The XRD, XPS, Cu L3VV signal, and FTIR spectra of the samples: (a) the XRD of lignin nanospheres and $\text{Cu}_2\text{O}@L$: (a-1) XRD of lignin nanospheres, (a-2) $\text{Cu}_2\text{O}@L$, and (a-3) fourth-time-reused $\text{Cu}_2\text{O}@L$; (b) the XPS and Cu L3VV signal of $\text{Cu}_2\text{O}@L$; (c) Cu 2p XPS spectrum peaks of $\text{Cu}_2\text{O}@L$; (d) the FTIR spectra of lignin and lignin nanosphere-based catalyst: (d-1) raw lignin, (d-2) lignin nanospheres, and (d-3) $\text{Cu}_2\text{O}@L$.

XPS and Cu L3VV Auger line results for Cu₂O@L were studied to investigate the components of the catalyst and the chemical state of the Cu element. The XPS complete spectra shows C 1s, O 1s, and Cu 2p peaks (Figure 4b). The result illustrates that there are C, O, and Cu elements in Cu₂O@L, corresponding with the EDS result. The binding energies of the Cu 2p of Cu₂O@L are located at 932.5 and 952.5 eV. In addition, there is a satellite peak at 944.6 eV in the XPS spectrum of the Cu 2p of the Cu₂O@L (Figure 4c). Furthermore, it is found that the peak of the Cu L3VV signals is centered at 916.8 eV, indicating the primary existence of Cu(I) in the catalyst [44]. According to the HRTEM, XRD, and XPS results, the nanoparticles on electrospayed lignin nanospheres are calculated to be Cu₂O.

Moreover, the structural characteristics of Cu₂O@L were investigated by FTIR spectrum. Figure 4d-1 shows the FTIR spectra of lignin. The characteristic FTIR absorption peaks of alkali lignin (from poplar) are 1327 cm⁻¹, 1269 cm⁻¹, and 1115 cm⁻¹ that are related to guaiacyls, the stretching vibrations of carbon–oxygen bonds, and ether bonds, respectively. The peaks at 3390 cm⁻¹, 1216 cm⁻¹, 1515 cm⁻¹, and 557 cm⁻¹ are attributed to phenolic hydroxyl groups, carbon double bonds of benzene, and acyl-oxygen bonds, respectively [45]. As shown in Figure 4d-2, the FTIR spectrum of the electrospayed lignin nanospheres is similar to that of lignin. Figure 4d-3 shows the FTIR spectrum of Cu₂O@L. The peak at 3390 cm⁻¹ shifts to 3379 cm⁻¹, and the peak at 1216 cm⁻¹ weakens, indicating interaction of phenolic hydroxyl and cuprous groups. As compared with lignin and lignin nanospheres, the peak at 1705 cm⁻¹ disappears in the FTIR spectrum of Cu₂O@L. This was probably due to the weakened π bond of carbon and oxygen resulting from interaction of cuprous and carbon–oxygen bonds. There are also some differences in the fingerprint region. The characteristic peak at 628 cm⁻¹ may be attributed to Cu₂O, which is caused by the overlap of the peak the 632 cm⁻¹ from lignin and the peak of 624 cm⁻¹ from Cu₂O.

Furthermore, thermal stabilities of the lignin nanospheres and Cu₂O@L were displayed in Figure S3. The lignin nanospheres and the catalyst have similar thermal properties, in that both of them show decomposition temperatures above 150 °C. Because the Huisgen [3+2] cycloaddition reactions in this study were carried out at room temperature, the thermal properties of Cu₂O@L could fully meet the temperature requirement of the reaction.

3.2. Catalytic Performance of Lignin Nanosphere-Supported Catalyst in the Huisgen “Click” Reaction

Solvent-free conditions confer to the reaction process simple operation, easy separation, and reduced environmental hazards [46]. With the aim to develop a “green” method for “click” chemistry, we attempted to synthesize triazoles under solvent-free conditions. The result is inspiring. As shown in Table S1, the reaction yield is almost 99% under solvent-free conditions without adding any base (with 1.2 mol % catalyst). The reason for this is that Cu₂O@L may achieve better contact with reaction reagents in such a situation. The product is able to crystallize out from the reactants during the reaction process, and the whole reaction can be monitored visually under the solvent-free condition. Moreover, different solvents, such as water, alcohol and, methanol have also been adopted as solvents for the reaction of benzyl azide and phenylacetylene. As compared with the solvent-free condition, the reaction yields are slightly lower than those of the other solvents using Cu₂O@L.

The classic cycloaddition reaction of benzyl azide and phenylacetylene was used to explore the optimum condition of the reaction. The results were encouraging, noting that the reaction between benzyl azide and phenylacetylene could be completed within 3 h under the solvent-free condition at ambient temperature. The effect of the Cu₂O@L quantity on the reaction was investigated. The reaction almost did not take place under the solvent-free condition at room temperature even after 24 h of stirring without the catalyst. When 0.6 mol % Cu₂O@L was used, the productivity reached 93%. The reaction could be completed in 3 h and provided a quantitative yield of the desired product with Cu₂O@L. The optimized result (99% yield) was obtained within 3 h under the solvent-free condition at room temperature with 1.2 mol % Cu₂O@L, while the yield of the reaction was only 27% and 25% using equivalent Cu₂O nanoparticles as the catalyst under the solvent-free condition or using H₂O as the solvent, respectively. Besides, the reaction did not take place when the lignin nanospheres were used alone.

After establishment of the optimum condition for the cycloaddition of benzyl azide and phenyl acetylene, a series of azides and terminal alkynes were further subjected to the Huisgen “click” reactions using $\text{Cu}_2\text{O}@L$ at room temperature under the solvent-free condition to further evaluate the efficiency of this methodology. The products obtained have been tabulated in Table 1. All the reactions could be completed within 3 h to give high yields of the corresponding 1,4-triazoles. The substituents of phenyl acetylene (electron-withdrawing, electron-rich, and heterocyclic) had no effect on the reaction, and tolerance for variations in the azide component was also excellent. In particular, the catalyst was very effective for aliphatic alkynes as well, and we could isolate 97% of the product between 4-nitrobenzyl azide and 1-hexyne.

Table 1. Huisgen “click” reactions using $\text{Cu}_2\text{O}@L$.

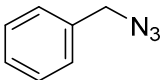
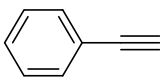
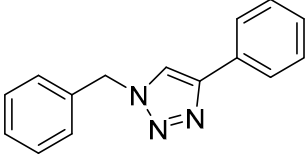
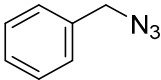
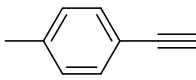
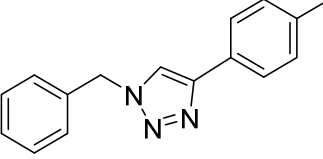
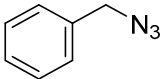
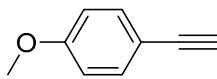
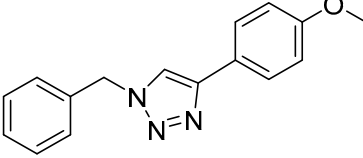
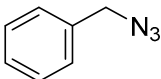
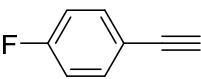
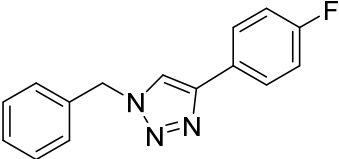
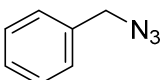
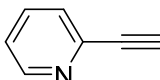
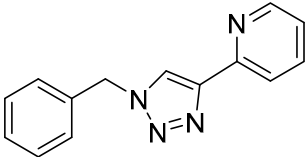
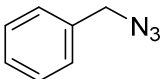
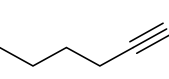
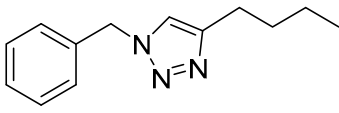
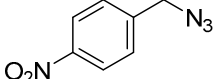
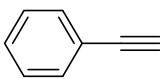
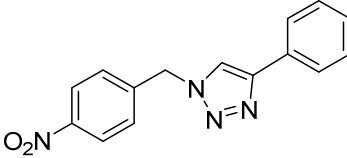
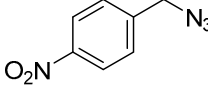
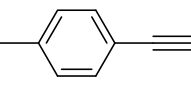
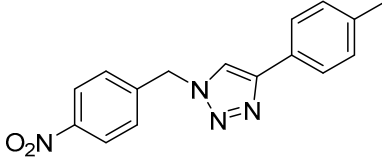
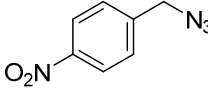
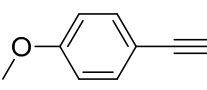
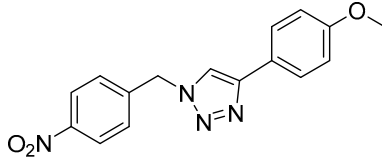
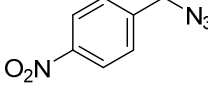
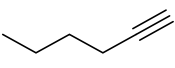
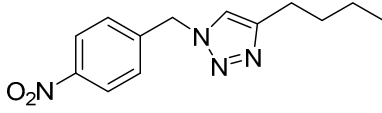
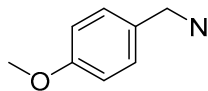
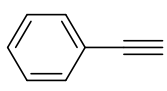
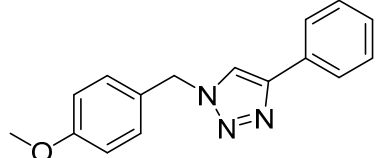
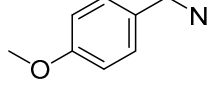
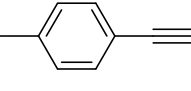
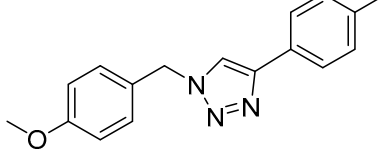
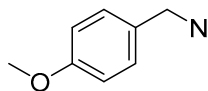
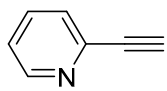
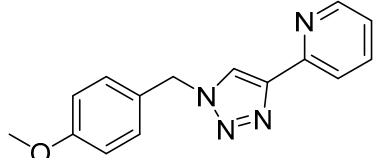
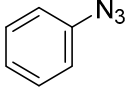
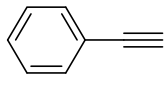
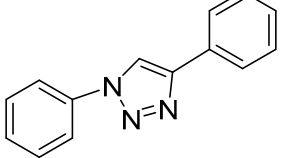
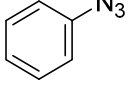
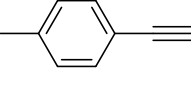
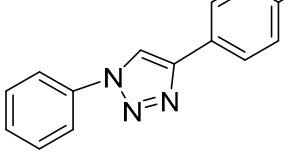
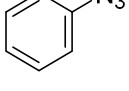
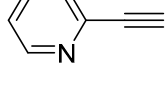
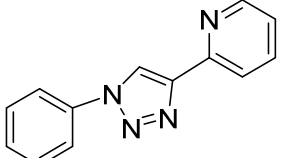
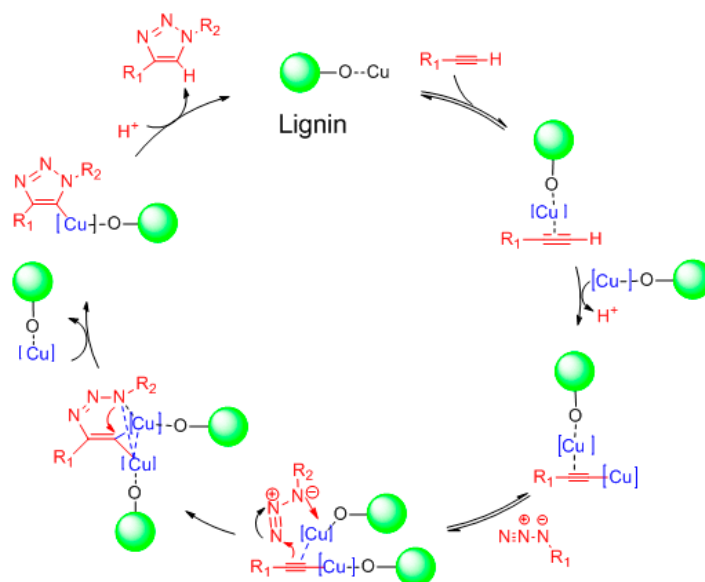
Reaction	Alkyl Halide	Alkyne	Product ^{a,b}	Yield (%) ^c
1				99
2				98
3				98
4				98
5				99
6				98
7				97

Table 1. Cont.

Reaction	Alkyl Halide	Alkyne	Product ^{a,b}	Yield (%) ^c
8				96
9				99
10				97
11				98
12				98
13				99
14				96
15				98
16				99

^a Reaction conditions: 1.0 mmol of alkyl azide, 1.2 mmol of alkyne, 1.2 mol % of Cu₂O@L, solvent-free, room temperature, 3 h, under air condition. ^b Products were characterized using NMR and compared with the reported data. ^c Isolated yield, according to mol of alkyl azide.

The possible mechanism for the catalytic cycle is proposed in Scheme 1, in which the whole reaction process is related to two copper atoms. In our work, Cu(I) is also considered to be the most active species. Cu(I) coordinates with strongly polar phenolic hydroxyl groups in lignin molecules and can form $\text{Cu}_2\text{O}@L$ coordination compounds. Then, there is the formation of $\text{Cu}_2\text{O}@L$ -acetylidine composites by initial coordination with alkynes. The $\text{Cu}_2\text{O}@L$ -acetylidine composites are added to azide groups to form the active cycloaddition composites. Finally, the cycloaddition composites give 1,2,3-triazole.



Scheme 1. The proposed catalytic mechanism for the “click” reaction catalyzed by $\text{Cu}_2\text{O}@L$ (red colors are from reactants and green colors are from catalyst).

4. Discussion

Cu(I) has always been considered to be one of the most active species in “click” chemistry. In this work, the catalytic active center of $\text{Cu}_2\text{O}@L$ is monovalent copper. Furthermore, the lignin nanosphere support has improved the catalytic activity of the Cu_2O nanoparticles for the yield of Huisgen “click” reactions, attributed to the formation of $\text{Cu}_2\text{O}@L$ composites (Figure S4). Therefore, the lignin nanosphere support can further provide sufficient catalytic active sites, which favors the continuation of the azide–alkyne cycloaddition reaction. These may be the reasons why all the yields of the products are impressive under the solvent-free condition at room temperature using $\text{Cu}_2\text{O}@L$. A comparison of some selected protocols in the literature and our method are listed in Table 2. The catalyst system was also characterized by electrochemistry (Figure S5).

$\text{Cu}_2\text{O}@L$ could be reused for four times without obvious change in its activity. As shown in Figure S6a, it can be observed that with the increasing number of cycles of the reaction, the catalytic activity of the catalyst does not decrease significantly. The $\text{Cu}_2\text{O}@L$ works extremely well even up to four subsequent cycles with 95% yield. These observations suggest that after few cycles, the catalytic efficiency can be preserved, which is attributed to the stable structure of $\text{Cu}_2\text{O}@L$. Metal leaching was studied by AAS analysis of the catalyst before and after four reaction cycles. The Cu element concentration is found to be 7.76% before the reaction and 7.62% after the reaction. The XRD result shows that there are still diffraction peaks in the reused catalyst (Figure 4a-3). The morphology of $\text{Cu}_2\text{O}@L$ after four cycles was investigated as well, as shown in Figure S6b,c. It is clearly shown that the Cu_2O nanoparticles still remain irregular in shape and dispersed uniformly on the surface of the lignin nanospheres. The XRD and TEM results indicate that the lignin nanosphere is a favorable support for cuprous oxide to catalyze Huisgen [3+2] cycloaddition reactions.

Table 2. The brief comparison of this catalyst with previous ones for Huisgen “click” reactions of azides and alkynes.

Entry	Catalyst	mol % ^a	Solvent	T (°C)	Time (h)	Yield (%)	Ref.
1	Copper in charcoal	5	dioxane	25	10	84	[47]
2	Copper in zeolite	10	toluene	25	15	94	[48]
3	CuSO ₄ ·5H ₂ O	1	H ₂ O/t-BuOH	90	8	89	[49]
4	Photocatalytic-Cu(II)	5	ethanol	25	5	96	[50]
5	Dendrimer-CuI	0.5	H ₂ O	25	3	98	[51]
6	Chitosan-CuSO ₄	0.4	H ₂ O	25	4–6	99	[8]
7	Cu on chelated resins	1	solvent-free	50/80	24/4	100	[52]
8	CuCl/microwaves	2.5	glycerol	100	0.5	82	[53]
9	CuOAc/ball-milling	10	solvent-free	-	1	90	[54]
10	CuO@Nb ₂ O ₅ /UV	1–1.2	THF	25	6	99	[55]
11	Cu ₂ O Nanocrystals	6.25	EtOH	55	1	96	[56]
12	Cu ₂ O@L	1.2	solvent-free	25	3	99	This work

^a Catalyst additive amount, mol %.

5. Conclusions

In summary, we developed a facile and powerful method to prepare Cu₂O@L using widely available and sustainable lignin by electro spraying technology. Alkali lignin was successfully processed into uniform nanospheres when electro spraying lignin precursor solution at an appropriate concentration under a determined voltage condition. The lignin nanosphere was further exploited as part of a high-performance cuprous oxide heterogeneous catalyst, and the catalyst exhibited an excellent catalytic activity for the Huisgen “click” reaction under the solvent-free and mild conditions. As compared with other copper-mediated “click” reactions, reactions adopting the Cu₂O@L showed higher yield (up to 99%) and required shorter reaction time and relatively mild conditions to synthesize 1,2,3-triazoles. The preparation process of the catalyst is economical, facile, and can be implemented on a large scale. In general, this work provided a “green” method for “click” chemistry and an efficient approach for application of the biomass resource lignin.

Supplementary Materials: The following are available online at <http://www.mdpi.com/2073-4360/10/7/724/s1>, Figure S1: SEM images of electro sprayed lignin from various concentrations of lignin solutions: (a) 25%, (b) 35%, (c) 45%, and (d) 55%, respectively; Figure S2: Particle size distribution of Cu₂O@L; Figure S3: The TGA of lignin and Cu₂O@L: (a) raw lignin, (b) lignin nanospheres, and (c) Cu₂O@L, respectively; Figure S4: The XPS spectrum of lignin nanospheres and Cu₂O@L: (a) lignin nanospheres, (b) Cu₂O@L, (c) O 1s XPS peaks of lignin nanospheres, (d) O1s XPS peaks of Cu₂O@L, (e) C 1s XPS peaks of lignin nanospheres, (f) C 1s XPS peaks of Cu₂O@L, (g) Cu 2p XPS spectrum of Cu₂O nanoparticles, (h) Cu2p XPS spectrum of Cu₂O@L, (i) XPS spectrum and Cu L3VV Auger line of lignin nanospheres as a reductant to prepare Cu₂O@Lignin, respectively; Figure S5: Recycling experiment and TEM images of Cu₂O@L: (a) Recycling experiment of Cu₂O@L, (b) fresh Cu₂O@L, and (c) the fourth-time-recycled Cu₂O@L, respectively; Figure S6: Recycling experiment and TEM images of Cu₂O@L: (a) Recycling experiment of Cu₂O@L, (b) fresh Cu₂O@L, and (c) the fourth-time-recycled Cu₂O@L, respectively; Scheme S1. Chemical equation of preparing Cu₂O@Lignin with lignin as an assistant reducing agent; Table S1. Effect of polarity of solvent on Huisgen “click” reaction of azides and alkynes using Cu₂O@L in different solvents; Spectroscopic data, 1H and 13C NMR Spectra of products.

Author Contributions: X.P. and R.S. conceived and designed the experiments; Z.Z. performed the experiments and wrote the paper; L.Z. and X.L. analyzed the data.

Acknowledgments: We wish to thank the National Natural Science Foundation of China (21336002, 31430092, 21506068), Guangdong Natural Science Funds for Distinguished Young Scholar (2016A030306027, 2017A030306029), Tip-top Scientific and Technical Innovative Youth Talents of Guangdong Special Support Program (2015TQ01C488), State Key Laboratory of Pulp and Paper Engineering and Fundamental Research Funds for the Central Universities.

Conflicts of Interest: The authors declare no conflict of interest.

Abbreviations

XRD	X-ray powder diffraction
SEM	Scanning electron microscopy
TEM	Transmission electron microscopy
XPS	X-ray photoelectron spectroscopy
AFM	Atomic force microscope
LSCM	Laser scanning confocal microscope
EDS	Energy dispersive analysis system of X-ray
TGA	Thermogravimetric analysis
FT-NMR	Fourier transform nuclear magnetic resonance
UV-vis-NIR	UV-visible-near infrared spectroscopy
FTIR	Fourier transformation infrared spectroscopy
AAS	Atomic absorption spectrophotometry
Cu ₂ O@L	the lignin nanosphere-supported cuprous oxide
DMF	<i>N,N</i> -dimethylformamide
ID	inner diameter
FL	Fluorescence spectra
PMT	Photomultiplier tube
M _w	weight-average molecular weight
TMS	tetramethylsilane

References

1. Kolb, H.C.; Finn, M.G.; Sharpless, K.B. Click Chemistry: Diverse Chemical Function from a Few Good Reactions. *Angew. Chem. Int. Ed.* **2001**, *40*, 2004–2021. [[CrossRef](#)]
2. Kumar, A.; Aerry, S.; Saxena, A.; Arnab, D.; Mozumdar, S. Copper nanoparticulates in Guar-gum: A recyclable catalytic system for the Huisgen [3+2]-cycloaddition of azides and alkynes without additives under ambient conditions. *Green Chem.* **2012**, *14*, 1298–1301. [[CrossRef](#)]
3. Yao, B.; Hu, T.; Zhang, H.; Li, J.; Sun, J.Z.; Qin, A.; Tang, B.Z. Multi-Functional Hyperbranched Poly(vinylene sulfide)s Constructed via Spontaneous Thiol–Yne Click Polymerization. *Macromolecules* **2015**, *48*, 7782–7791. [[CrossRef](#)]
4. Amblard, F.; Cho, J.H.; Schinazi, R.F. Cu(I)-catalyzed Huisgen azide-alkyne 1,3-dipolar cycloaddition reaction in nucleoside, nucleotide, and oligonucleotide chemistry. *Chem. Rev.* **2009**, *109*, 4207–4220. [[CrossRef](#)] [[PubMed](#)]
5. Baig, R.N.; Varma, R.S. Copper on chitosan: A recyclable heterogeneous catalyst for azide–alkyne cycloaddition reactions in water. *Green Chem.* **2013**, *15*, 1839–1843. [[CrossRef](#)]
6. Choudary, B.M.; Kantam, M.L.; Ranganath, K.V.; Mahendar, K.; Sreedhar, B. Bifunctional Nanocrystalline MgO for Chiral Epoxy Ketones via Claisen–Schmidt Condensation–Asymmetric Epoxidation Reactions. *J. Am. Chem. Soc.* **2004**, *126*, 3396–3397. [[CrossRef](#)] [[PubMed](#)]
7. Yin, L.; Liebscher, J. Carbon–Carbon Coupling Reactions Catalyzed by Heterogeneous Palladium Catalysts. *Chem. Rev.* **2007**, *107*, 133–173. [[CrossRef](#)] [[PubMed](#)]
8. Alonso, F.; Moglie, Y.; Radivoy, G. Copper Nanoparticles in Click Chemistry. *Chem. Res.* **2015**, *48*, 2516–2528. [[CrossRef](#)] [[PubMed](#)]
9. Lee, S.H.; Yu, S.; Shahzad, F.; Hong, J.P.; Kim, W.N.; Park, C.; Soon, M.H.; Koo, C.M. Highly anisotropic Cu oblate ellipsoids incorporated polymer composites with excellent performance for broadband electromagnetic interference shielding. *Compos. Sci. Technol.* **2017**, *144*, 57–62. [[CrossRef](#)]
10. Jumde, R.P.; Evangelisti, C.; Mandoli, A.; Scotti, N.; Psaro, R. Aminopropyl-silica-supported Cu nanoparticles: An efficient catalyst for continuous-flow Huisgen azide-alkyne cycloaddition (CuAAC). *J. Catal.* **2015**, *324*, 25–31. [[CrossRef](#)]
11. Gu, L.; Ma, D.; Yao, S.; Wang, C.; Shen, W.; Bao, X. Structured zeolite catalysts with hierarchical channel structure. *Chem. Commun.* **2010**, *46*, 1733–1735. [[CrossRef](#)] [[PubMed](#)]

12. Zhang, S.; Gao, W.; Li, J.; Zhou, X.; Qu, Y. Interfacial Effects of the CuO/GO Composite to Mediate the Side Reactions of *N,N*-Dimethylformamide Fragments. *ACS Appl. Mater. Interfaces* **2014**, *6*, 22174–22182. [[CrossRef](#)] [[PubMed](#)]
13. Suresh Kumar, B.; Amali, A.J.; Pitchumani, K. Fabrication of Pd Nanoparticles Embedded C@Fe₃O₄ Core–Shell Hybrid Nanospheres: An Efficient Catalyst for Cyanation in Aryl Halides. *ACS Appl. Mater.* **2015**, *7*, 22907–22917. [[CrossRef](#)] [[PubMed](#)]
14. Madhavan, N.; Jones, C.W.; Weck, M. Rational Approach to Polymer-Supported Catalysts: Synergy between Catalytic Reaction Mechanism and Polymer Design. *Acc. Chem. Res.* **2008**, *41*, 1153–1165. [[CrossRef](#)] [[PubMed](#)]
15. Zhou, Z.; Peng, X.; Zhong, L.; Wu, L.; Cao, X.; Sun, R.C. Electrospun cellulose acetate supported Ag@AgCl composites with facet-dependent photocatalytic properties on degradation of organic dyes under visible-light irradiation. *Carbohydr. Polym.* **2016**, *136*, 322–328. [[CrossRef](#)] [[PubMed](#)]
16. Tzounis, L.; Contreras-Caceres, R.; Schellkopf, L.; Jehnichen, D.; Fischer, D.; Cai, C.; Stamm, M. Controlled growth of Ag nanoparticles decorated onto the surface of SiO₂ spheres: A nanohybrid system with combined SERS and catalytic properties. *RSC Adv.* **2014**, *4*, 17846–17855. [[CrossRef](#)]
17. Papageridis, K.N.; Siakavelas, G.; Charisiou, N.D.; Avraam, D.G.; Tzounis, L.; Kousi, K.; Goula, M.A. Comparative study of Ni, Co, Cu supported on γ -alumina catalysts for hydrogen production via the glycerol steam reforming reaction. *Fuel Process. Technol.* **2016**, *152*, 156–175. [[CrossRef](#)]
18. Tzounis, L.; Logothetidis, S. Fe₃O₄@SiO₂ core shell particles as platforms for the decoration of Ag nanoparticles. *Mater. Today Proc.* **2017**, *4*, 7076–7082. [[CrossRef](#)]
19. Charisiou, N.D.; Siakavelas, G.; Papageridis, K.N.; Baklavariadis, A.; Tzounis, L.; Avraam, D.G.; Goula, M.A.J. Sorbent-Enhanced Methane Reforming over a Ni–Ca-Based, Bifunctional Catalyst Sorbent. *Nat. Gas Sci. Eng.* **2016**, *31*, 164–183. [[CrossRef](#)]
20. Goula, M.A.; Charisiou, N.D.; Siakavelas, G.; Tzounis, L.; Tsiaoussis, I.; Panagiotopoulou, P.; Yentekakis, I.V. Syngas production via the biogas dry reforming reaction over Ni supported on zirconia modified with CeO₂ or La₂O₃ catalysts. *J. Hydrog. Energy* **2017**, *42*, 13724–13740. [[CrossRef](#)]
21. Charisiou, N.D.; Papageridis, K.N.; Tzounis, L.; Sebastian, V.; Hinder, S.J.; Baker, M.A.; Goula, M.A. Ni supported on CaO–MgO–Al₂O₃ as a highly selective and stable catalyst for H₂ production via the glycerol steam reforming reaction. *Int. J. Hydrog. Energy* **2018**. [[CrossRef](#)]
22. Szczyrek, A.; Fierro, V.; Pizzi, A.; Stauber, M.; Celzard, A. Corrigendum to “A new method for preparing tannin-based foams”. *Ind. Crops Prod.* **2015**, *67*, 510. [[CrossRef](#)]
23. Da Silva Souza, D.R.; de Mesquita, J.P.; Lago, R.M.; Caminhas, L.D.; Pereira, F.V. Cellulose nanocrystals: A versatile precursor for the preparation of different carbon structures and luminescent carbon dots. *Ind. Crops Prod.* **2016**, *93*, 121–128. [[CrossRef](#)]
24. Si, H.; Lian, G.; Wang, J.; Li, L.; Wang, Q.; Cui, D.; Wong, C.P. Synthesis of Few-Atomic-Layer BN Hollow Nanospheres and Their Applications as Nanocontainers and Catalyst Support Materials. *ACS Appl. Mater. Interfaces* **2016**, *8*, 1578–1582. [[CrossRef](#)] [[PubMed](#)]
25. Carrott, P.J.M.; Carrott, M.R. Lignin—From natural adsorbent to activated carbon: A review. *Bioresour. Technol.* **2007**, *98*, 2301–2312.
26. Wang, S.X.; Yang, L.; Stubbs, L.P.; Li, X.; He, C. Lignin-Derived Fused Electrospun Carbon Fibrous Mats as High Performance Anode Materials for Lithium Ion Batteries. *ACS Appl. Mater. Interfaces* **2013**, *5*, 12275–12282. [[CrossRef](#)] [[PubMed](#)]
27. Kadla, J.F.; Kubo, S.; Venditti, R.A.; Gilbert, R.D.; Compere, A.L.; Griffith, W. Lignin-based carbon fibers for composite fiber applications. *Carbon* **2002**, *40*, 2913–2920. [[CrossRef](#)]
28. Graglia, M.; Pampel, J.; Hantke, T.; Fellinger, T.P.; Esposito, D. Nitro Lignin-Derived Nitrogen-Doped Carbon as an Efficient and Sustainable Electrocatalyst for Oxygen Reduction. *ACS Nano* **2016**, *10*, 4364–4371. [[CrossRef](#)] [[PubMed](#)]
29. Li, Y.; Wu, Y.; Zeng, W.; Li, Y.; Xu, L.; Qiu, X.; Chen, R.F.; Huang, W. Improving Efficiency of Blue Organic Light-Emitting Diode with Sulfobutylated Lignin Doped PEDOT as Anode Buffer Layer. *ACS Sustain. Chem. Eng.* **2016**, *4*, 2004–2011. [[CrossRef](#)]
30. Chung, H.; Washburn, N.R. Chemistry of lignin-based materials. *Green Mater.* **2013**, *1*, 137–160. [[CrossRef](#)]

31. Ralph, J.; Lundquist, K.; Brunow, G.; Lu, F.; Kim, H.; Schatz, P.F.; Jørgen, H.C.; Boerjan, W. Lignins: Natural polymers from oxidative coupling of 4-hydroxyphenyl-propanoids. *Phytochem. Rev.* **2004**, *3*, 29–60. [[CrossRef](#)]
32. Boerjan, W.; Ralph, J.; Baucher, M. Lignin biosynthesis. *Annu. Rev. Plant Biol.* **2003**, *54*, 519–546. [[CrossRef](#)] [[PubMed](#)]
33. Vanholme, R.; Demedts, B.; Morreel, K.; Ralph, J.; Boerjan, W. Lignin biosynthesis and structure. *Plant Physiol.* **2010**, *153*, 895–905. [[CrossRef](#)] [[PubMed](#)]
34. Kai, D.; Jiang, S.; Low, Z.W.; Loh, X.J. Engineering highly stretchable lignin-based electrospun nanofibers for potential biomedical applications. *J. Mater. Chem. B* **2015**, *3*, 6194–6204. [[CrossRef](#)]
35. Guo, X.; Zhang, S.; Shan, X.Q. Adsorption of metal ions on lignin. *J. Hazard. Mater.* **2008**, *151*, 134–142. [[CrossRef](#)] [[PubMed](#)]
36. Sud, D.; Mahajan, G.; Kaur, M.P. Agricultural waste material as potential adsorbent for sequestering heavy metal ions from aqueous solutions—A review. *Bioresour. Technol.* **2008**, *99*, 6017–6027. [[CrossRef](#)] [[PubMed](#)]
37. Shen, Z.G.; Luo, Y.Q.; Wang, Q.; Wang, X.Y.; Sun, R.C. High-Value Utilization of Lignin to Synthesize Ag Nanoparticles with Detection Capacity For Hg²⁺. *ACS Appl. Mater. Interfaces* **2014**, *6*, 16147–16155. [[CrossRef](#)] [[PubMed](#)]
38. Wang, Y.; Ren, K.; Sun, J.; Li, W.; Zhao, S.; Chen, Z.; Guan, J. Ultralow content silver densely-coated glass microsphere for high performance conducting polymer-matrix composites. *Compos. Sci. Technol.* **2017**, *140*, 89–98.
39. Lu, C.; Qi, L.; Yang, J.; Wang, X.; Zhang, D.; Xie, J.; Ma, J. One-Pot Synthesis of Octahedral Cu₂O Nanocages via a Catalytic Solution Route. *Adv. Mater.* **2005**, *17*, 2562–2567. [[CrossRef](#)]
40. Xue, Y.; Qiu, X.; Wu, Y.; Qian, Y.; Zhou, M.; Deng, Y.; Li, Y. Aggregation-induced emission: The origin of lignin fluorescence. *Polym. Chem.* **2016**, *7*, 3502–3508. [[CrossRef](#)]
41. Hong, N.; Xiao, J.; Li, Y.; Li, Y.; Wu, Y.; Yu, W.; Cao, Y. Unconventional fluorescence emission of non-conjugated lignin-SAF (GSL) was reported and GSL-doped PEDOT showed high performance in organic electronics. *J. Mater. Chem. C* **2016**, *4*, 5297–5306. [[CrossRef](#)]
42. Park, J.C.; Kim, J.; Kwon, H.; Song, H. Gram-Scale Synthesis of Cu₂O Nanocubes and Subsequent Oxidation to CuO Hollow Nanostructures for Lithium-Ion Battery Anode Materials. *Adv. Mater.* **2009**, *21*, 803–807. [[CrossRef](#)]
43. Jiao, S.; Xu, L.; Jiang, K.; Xu, D. Well-Defined Non-spherical Copper Sulfide Mesocages with Single-Crystalline Shells by Shape-Controlled Cu₂O Crystal Templating. *Adv. Mater.* **2006**, *18*, 1174–1177. [[CrossRef](#)]
44. Yang, W.Y.; Rhee, S.W. Effect of electrode material on the resistance switching of Cu₂O film. *Appl. Phys. Lett.* **2007**, *91*, 232907. [[CrossRef](#)]
45. Xiao, B.; Sun, X.F.; Sun, R.C. Chemical, structural, and thermal characterizations of alkali-soluble lignins and hemicelluloses, and cellulose from maize stems, rye straw, and rice straw. *Polym. Degrad. Stab.* **2001**, *74*, 307–319. [[CrossRef](#)]
46. Luo, R.; Zhou, X.; Fang, Y.; Ji, H. Metal-and solvent-free synthesis of cyclic carbonates from epoxides and CO₂ in the presence of graphite oxide and ionic liquid under mild conditions: A kinetic study. *Carbon* **2015**, *82*, 1–11. [[CrossRef](#)]
47. Lipshutz, B.H.; Taft, B.R. Heterogeneous Copper-in-Charcoal-Catalyzed Click Chemistry. *Angew. Chem. Int. Ed.* **2006**, *118*, 8415–8418. [[CrossRef](#)]
48. Chassaing, S.; Kumarraja, M.; Sani Souna Sido, A.; Pale, P.; Sommer, J. Click Chemistry in CuI-zeolites: The Huisgen [3+2]-Cycloaddition. *Org. Lett.* **2007**, *9*, 883–886. [[CrossRef](#)] [[PubMed](#)]
49. Rostovtsev, V.V.; Green, L.G.; Fokin, V.V.; Sharpless, K.B. A Stepwise Huisgen Cycloaddition Process: Copper(I)-Catalyzed Regioselective “Ligation” of Azides and Terminal Alkynes. *Angew. Chem. Int. Ed.* **2002**, *114*, 2708–2711. [[CrossRef](#)]
50. Kumar, P.; Joshi, C.; Srivastava, A.K.; Gupta, P.; Boukherroub, R.; Jain, S.L. Visible Light Assisted Photocatalytic [3+2] Azide–Alkyne “Click” Reaction for the Synthesis of 1,4-Substituted 1,2,3-Triazoles Using a Novel Bimetallic Ru–Mn Complex. *ACS Sustain. Chem. Eng.* **2015**, *4*, 69–75. [[CrossRef](#)]
51. Deraedt, C.; Pinaud, N.; Astruc, D. Recyclable Catalytic Dendrimer Nanoreactor for Part-Per-Million Cu^I Catalysis of “Click” Chemistry in Water. *J. Am. Chem. Soc.* **2014**, *136*, 12092–12098. [[PubMed](#)]

52. Monguchi, Y.; Nozaki, K.; Maejima, T.; Shimoda, Y.; Sawama, Y.; Kitamura, Y.; Kitade, Y.; Sajiki, H. Solvent-free Huisgen cyclization using heterogeneous copper catalysts supported on chelate resins. *Green Chem.* **2013**, *15*, 490–495.
53. Rodríguez-Rodríguez, M.; Gras, E.; Pericàs, M.A.; Gómez, M. Metal-Free Intermolecular Azide–Alkyne Cycloaddition Promoted by Glycerol. *Chemistry* **2015**, *21*, 18706–18710. [[CrossRef](#)] [[PubMed](#)]
54. Chen, X.; Jia, C.; Cao, L.; Zhang, D.; Liu, S.; Zhang, Q. Solvent-free 1,3-dipolar cycloaddition of azomethine imines with terminal alkynes promoted by calcium fluoride under the ball milling condition. *Chem. Res. Chin. Univ.* **2015**, *31*, 543–548. [[CrossRef](#)]
55. Wang, B.; Durantini, J.; Nie, J.; Lanterna, A.E.; Scaiano, J.C. Heterogeneous Photocatalytic Click Chemistry. *J. Am. Chem. Soc.* **2016**, *138*, 13127–13130. [[CrossRef](#)] [[PubMed](#)]
56. Chanda, K.; Rej, S.; Huang, M.H. Facet-Dependent Catalytic Activity of Cu. *Chemistry* **2013**, *19*, 16036–16043. [[CrossRef](#)] [[PubMed](#)]



© 2018 by the authors. Licensee MDPI, Basel, Switzerland. This article is an open access article distributed under the terms and conditions of the Creative Commons Attribution (CC BY) license (<http://creativecommons.org/licenses/by/4.0/>).